The Role of Fission in Mass Sensitivity Study of the *r*-process*

Yi Wei Hao[1,2] Yi Fei Niu[1,2†] Zhong Ming Niu[3]

[1]Frontier Science Center for Rare Isotope, Lanzhou University, Lanzhou 730000, China
[2]School of Nuclear Science and Technology, Lanzhou University, Lanzhou 730000, China
[3]School of Physics and Optoelectronic Engineering, Anhui University, Hefei 230601, China

Abstract: A sensitivity study was performed to investigate the impact of individual nuclear masses on *r*-process rare-earth peak abundances in different astrophysical scenarios. The most impactful nuclei are primarily distributed in two regions on the nuclear chart: one located 20-30 neutrons away from stability (defined as region I) and another 7-15 neutrons away from stability (defined as region II), as previously reported in Phys. Lett. B 844, 138092 (2023). In this work, we extend our analysis by focusing on the role of fission in the mass sensitivity study. The results show that in astrophysical scenarios involving fission, the sensitivity of nuclei in region I is diminished due to the deposition of a large number of fission fragments in the rare-earth mass region. However, nuclei in region II retain high sensitivity because the contribution of fission decreases in the later stages of nucleosynthesis. This study highlights the impact of fission on the sensitivity of *r*-process abundances to nuclear masses and helps to enhance the understanding of the rare-earth peak formation mechanism.

Keywords: *r*-process, Rare-earth peak, Nuclear mass, Fission

DOI: 10.1088/1674-1137/adfe55 **CSTR:**

I. INTRODUCTION

The rapid neutron-capture process (*r*-process) is a fundamental mechanism in astrophysical nucleosynthesis, responsible for producing approximately half of the elements heavier than iron. This process occurs in extreme astrophysical environments with high neutron fluxes, enabling nuclei to undergo successive neutron captures before decaying back to stability [1]. Observations of metal-poor stars and meteorites reveal the characteristic abundance patterns of the *r*-process, highlighting its crucial role in cosmic chemical evolution [2]. However, despite decades of research, the exact astrophysical sites responsible for the *r*-process remain uncertain.

To unravel the origin of *r*-process elements, theoretical simulations of the nucleosynthesis process are necessary and rely on two essential input components: astrophysical conditions and nuclear properties. Both aspects introduce significant uncertainties. The astrophysical conditions, such as neutron flux, expansion timescale, temperature, and density evolution, all affect nucleosynthesis outcomes [3, 4]. Meanwhile, the nuclear properties of neutron-rich isotopes, such as masses, β-decay rates, neutron capture rates, fission rates, and fission yields, remain largely unmeasured and must be inferred from theoretical models, but these predictions often diverge [5−10]. These uncertainties hinder precise modeling of the *r*-process and complicate the interpretation of observed abundance patterns.

One of the unresolved questions in *r*-process nucleosynthesis is the formation mechanism of the rare-earth peak around mass number $A \sim 165$. Unlike the second and third *r*-process peaks, which are associated with closed neutron shells, the rare-earth peak is thought to originate from other nuclear structure effects [1, 11, 12]. The rare-earth peak could serve as a diagnostic tool for constraining astrophysical conditions of the *r*-process if its formation were well understood [13]. However, due to the large uncertainties in nuclear physics inputs, the abundance patterns obtained from *r*-process simulations exhibit large variance bands that exceed the peak itself, making it difficult to distinguish the abundance patterns produced by different astrophysical environments [6, 14−16]. To improve the reliability of such constraints, it is necessary to reduce uncertainties in nuclear physics inputs.

Received 31 March 2025; Accepted 18 August 2025

* This work was supported by the "Young Scientist Scheme" of National Key Research and Development (R&D) Program under grant No. 2021YFA1601500, the National Natural Science Foundation of China under grant Nos. 12075104, 12447168, 12447106, 11875070, 11935001 and 12375109, the China Postdoctoral Science Foundation (Grant No. 2025M773346), the Lingchuang Research Project of China National Nuclear Corporation (Grant No. CNNC-LCKY-2024-082), the Fundamental Research Funds for the Central Universities (lzujbky-2023-stlt01), the Anhui project (Z010118169), and the Key Research Foundation of Education Ministry of Anhui Province (2023AH050095). The authors also want to thank the fruitful discussions with Prof. F. Q. Chen and Dr. W. L. Lv.

† E-mail: E-mail: niuyf@lzu.edu.cn

Since it is challenging to experimentally measure the nuclear properties of a large number of neutron-rich nuclei, sensitivity studies provide an effective approach to pinpoint the key nuclei that have a significant impact on *r*-process abundances [6, 14−23]. The previous sensitivity studies have primarily focused on the global effects on the abundance distributions caused by mass variations, while the specific nuclei that affect the rare-earth peak formation remain unclear. So we performed sensitivity studies specifically targeting the rare-earth peak formation by individually modifying nuclear masses in the relevant region. We find the nuclei that have the most significant influence on the rare-earth peak are mainly distributed in two regions, as previously reported in Ref. [24]. However, in the astrophysical scenarios where a large number of fission events occur, the high sensitivity of nuclei lying along the *r*-process freeze-out path is diminished.

The present paper goes together with Ref. [24]. In this work, we have extended our analysis focusing on the role of fission in the sensitivity study of *r*-process abundances to nuclear masses. We analyzed in detail the reasons for the different distribution patterns of nuclei with high sensitivity under different astrophysical scenarios. Our results highlight the impact of fission in shaping the rare-earth peak abundances and help to enhance the understanding of the rare-earth peak formation mechanism as well as improve its effectiveness as a diagnostic for the *r*-process site.

II. *r*-PROCESS CALCULATIONS

The nuclear network NucNet [25] was used to simulate *r*-process nucleosynthesis. This network includes more than 6000 isotopes, covering nuclei with atomic number $Z \leq 102$. We take nuclear masses from the finite-range droplet model (FRDM) [26]. The neutron-capture rates are calculated with the publicly available statistical model code TALYS [27]. The β-decay rates are taken from the JINA REACLIB database [28]. Fission is included as in Ref. [29].

The *r*-process calculations were performed using a parameterized trajectory as implemented in Refs. [12, 13], where the density as a function of time is given by:

$$\rho(t) = \rho_1 \exp(-t/\tau) + \rho_2 \left(\frac{\Delta}{\Delta + t}\right)^n \quad (1)$$

where $\rho_1 + \rho_2$ is the density at time $t = 0$, τ is the expansion timescale, and Δ is a constant real number. The parameter n sets the thermodynamic behavior of the evolution at the late time of the *r*-process. For this work, we chose three distinct astrophysical scenarios: (1) a hot wind *r*-process with entropy 150 k_B, $Y_e = 0.3$, $\tau = 20$ ms, and $n = 2$, (2) a hot wind *r*-process with entropy 233 k_B, $Y_e = 0.1$, $\tau = 35$ ms, and $n = 2$, and (3) a cold wind *r*-process with entropy 150 k_B, $Y_e = 0.2$, $\tau = 20$ ms, and $n = 6$. In all scenarios, nucleosynthesis calculations start at an initial temperature $T = 10$ GK. We label these three trajectories as *hot1*, *hot2*, and *cold*, respectively.

In the *hot1* scenario, fission plays a negligible role in nucleosynthesis due to fewer neutrons in the environment, which prevents significant production of fissioning nuclei. In contrast, both the *hot2* and *cold* scenarios enable the formation of a substantial number of fissioning nuclei, leading to the deposition of numerous fission fragments in the $A = 110 \sim 170$ region. This is based on the GEF fission fragment distribution model [30], which predicts that fission yields in the neutron-rich regions exhibit both symmetric and asymmetric components [29, 31]. To isolate the effects of fission without direct contributions from fission fragments to the rare-earth peak, we conducted an additional set of simulations under the *cold* scenario. In these simulations, we imposed a simple symmetric split for fission product distributions, ensuring that the fission fragments mainly populate the $A \sim 130$ peak region instead of the rare-earth peak. This specific set of simulations is referred to as the *cold-sym* trajectory in the following discussion.

Following previous sensitivity studies [14, 18], we vary the mass of a single nucleus by ±1 MeV for 414 nuclei relevant to rare-earth peak formation [12]. For each variation, an abundance pattern is calculated and compared to the baseline using the sensitivity measure F,

$$F = 100 \sum_{A=150}^{178} \frac{|\, Y_{+1}(A) - Y_{ori.}(A) \,| + |\, Y_{-1}(A) - Y_{ori.}(A) \,|}{Y_{ori.}(A)}. \quad (2)$$

$Y_{ori.}(A)$ is the baseline abundance, and $Y_{+1}(A)$ and $Y_{-1}(A)$ are the abundances of the simulations where a single nuclear mass is increased or decreased by 1 MeV, respectively. When $Y_{ori.}(A)$, $Y_{+1}(A)$, and $Y_{-1}(A)$ are taken as the final abundances, the corresponding F-values can be found in Ref. [24]. In the present work, we further compute the sensitivity measure $F_{freeze-out}$ of the abundance distribution at freeze-out with respect to nuclear mass variations, where $Y_{ori.}(A)$, $Y_{+1}(A)$, and $Y_{-1}(A)$ refer to the abundances at the time of *r*-process freeze-out. This allows us to better understand how nuclear mass variations influence the abundance evolution prior to the onset of decay back to stability.

III. RESULTS AND DISCUSSIONS

Previous studies [11, 12] have suggested that the formation of the rare-earth peak occurs during the decay back to stability after the *r*-process freeze-out. In our earlier work [24], we further clarified that the rare-earth peak forms within the time interval between the *r*-pro-

cess freeze-out and the point when the neutron capture timescale ($\tau_{n\gamma}$) becomes approximately three times longer than the β-decay timescale (τ_β). At this moment, when $\tau_{n\gamma} \approx 3\tau_\beta$, the rare-earth peak abundances are already close to their final values, indicating that the peak has essentially formed by then. The nuclei that have the most significant influence on the rare-earth peak are mainly distributed in two regions. Region I, located 20-30 neutrons away from stability, corresponds to the position of the nuclear flow at *r*-process freeze-out. Region II, 7-15 neutrons away from stability, aligns with the *r*-process path at the point of $\tau_{n\gamma} \approx 3\tau_\beta$.

Fig. 1 shows the distribution of nuclei with high sensitivity measure F under different astrophysical scenarios,

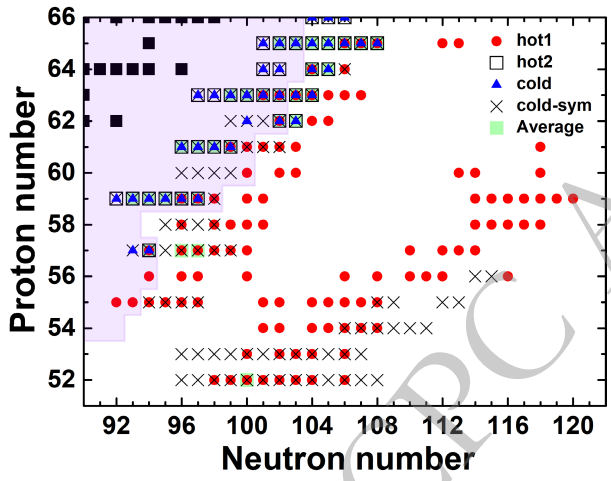

Fig. 1. (Color Online) Distribution of nuclei with sensitivity measure F greater than 200 in the *hot1*, *hot2*, *cold*, and *cold-sym* scenarios. The region of measured nuclear masses from AME2020 [32] is overlaid with pink color and solid black squares are stable isotopes. The data of sensitivity measure F in four different scenarios are taken from Ref. [24]. The top 30 nuclei with the largest averaged sensitivity F values across the *hot1*, *hot2*, and *cold* scenarios are indicated by light green shaded squares.

with the sensitivity data in four different scenarios taken from Ref. [24]. As a supplement to this analysis, we further calculate the average sensitivity measure F across the *hot1*, *hot2*, and *cold* scenarios. The top 30 nuclei with the largest averaged sensitivity F values are listed in Table 1 and are also indicated by light green shaded squares in Fig. 1. It is evident that the nuclei with the highest averaged sensitivity values are primarily located in region II, because these nuclei exhibit consistently high sensitivity across multiple astrophysical scenarios. In contrast, region I contains only one nucleus, ^{152}Te, with a relatively high averaged sensitivity. Although the sensitivity measure F of ^{152}Te is low under the *hot2* and *cold* scenarios, its exceptionally high sensitivity under the *hot1* scenario results in a large average F value.

In the scenarios considered here, the equilibrium phases are maintained at the time of *r*-process freeze-out. Thus, the final abundances are expected to be sensitive to changes in the masses of nuclei located along the *r*-process freeze-out path, as has been explained in detail in our previous work [24]. However, in the *hot2* and *cold* scenarios, the nuclei in region I exhibit lower F values, indicating that mass variations in this region have little or no impact on the final abundance distribution.

Nevertheless, we found that mass variations of certain nuclei in region I can lead to significant differences in the abundance pattern at the time of *r*-process freeze-out, as shown in Fig. 2. We selected two nuclei from region I as examples. In the *hot1* scenario, the mass variation of ^{152}Te results in a noticeable difference in the abundance distribution at the freeze-out time. In the cold scenario, the mass variation of ^{172}Ba also leads to significant differences at freeze-out. However, compared to the *hot1* case, the overall abundance in the rare-earth peak region is much lower. The situation in the *hot2* scenario is similar to the *cold* scenario. To quantify the sensitivity of the abundance distribution at freeze-out time to nuclear masses, we calculated the sensitivity measure $F_{freeze-out}$, which reflects how mass variations influence the abundance pattern at freeze-out. The results are

Table 1. The 30 most important nuclei with the highest averaged sensitivity measures F were obtained by averaging the F values across the *hot1*, *hot2*, and *cold* scenarios. An asterisk denotes a nucleus with experimental mass data in the AME2020 mass table [32]. A detailed list of the nuclei with the highest sensitivity under each astrophysical scenario is available in Ref. [24].

Average														
Z	*A*	*F*	*Z*	*A*	*F*	*Z*	*A*	*F*	*Z*	*A*	*F*	*Z*	*A*	*F*
64	168	412.73	63	165	348.09*	65	168	301.85*	63	163	273.11*	65	167	233.27*
63	166	396.32	61	159	317.41*	57	153	301.48	59	156	268.38*	52	152	232.14
65	170	386.57	62	164	315.41*	59	155	296.77*	59	154	265.96*	59	152	229.16*
63	164	377.39*	65	172	312.50	65	171	295.67	63	162	259.27*	59	153	222.69*
65	169	376.35	61	158	306.86*	65	173	282.38	57	151	245.65*	62	165	220.96
63	167	349.18	64	169	306.86	57	154	273.65	61	160	240.01*	61	157	220.32*

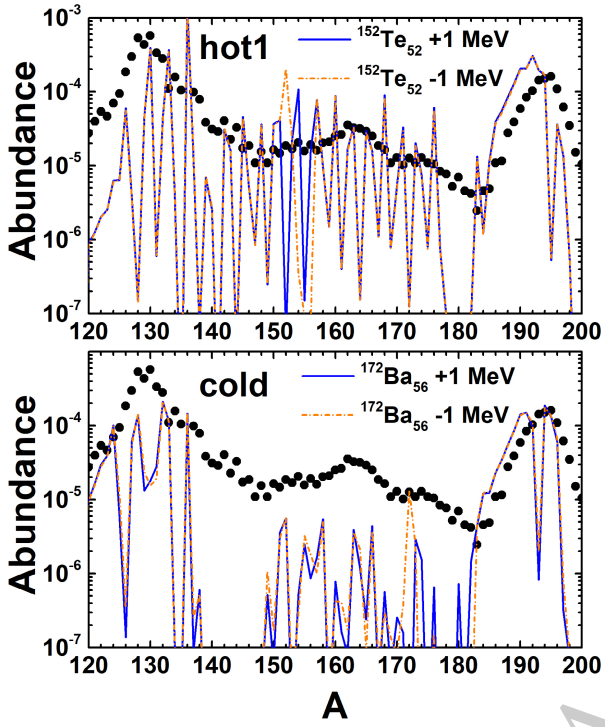

Fig. 2. (Color Online) Abundance distributions at the time of *r*-process freeze-out after nuclear mass variation in the *hot1* and *cold* scenarios. The solid blue line represents the abundance distribution resulting from a mass increase of 1 MeV, while the dotted orange line corresponds to the abundance distribution resulting from a mass decrease of 1 MeV. The dots represent the solar *r*-process abundance pattern [33].

presented in Fig. 3 and 4, where the left panels display the sensitivity measures, and the right panels present the corresponding abundance distributions at *r*-process freeze-out. The results indicate that, in the four scenarios considered here, region I corresponds to the region through which the nuclear flow passes at freeze-out. In the *cold* scenario, the nuclear flow extends farther from stability compared to the hot *r*-process conditions. It can be clearly seen that nuclei with high sensitivity are distributed along the *r*-process freeze-out path, implying that mass variations of nuclei in this region strongly impact the abundance distribution at freeze-out across all four scenarios.

In the *hot1* scenario, differences in the abundance distribution at freeze-out propagate through the later stage of nucleosynthesis, leading to significant variations in the final abundance pattern. However, in the *hot2* and *cold* scenarios, even though mass variations of certain nuclei in region I cause considerable differences in the abundance distribution at freeze-out, their impact on the final abundance pattern is minimal or negligible. This is primarily due to the influence of fission fragments, which play an important role in shaping the rare-earth peak abundances. We calculated the contribution of fission products to the abundance in the *cold* scenario as an example to prove this point, which is defined as

$$\Delta Y_{Fragment}(A) = \sum_n \sum_i f_i^{(n)} \times w_i(A). \quad (3)$$

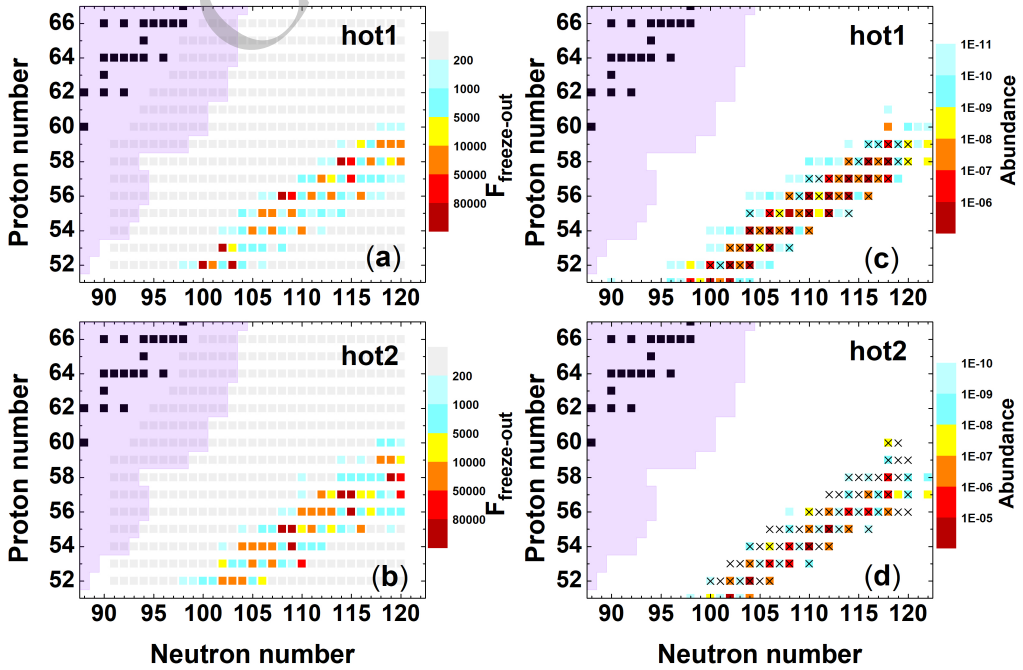

Fig. 3. (Color Online) In the *hot1* and *hot2* scenarios, panels (a) and (b) correspond to the sensitivity measure $F_{freeze-out}$ of the abundance distribution at *r*-process freeze-out to nuclear masses, and panels (c) and (d) correspond to the abundance distribution patterns at freeze-out. Nuclei with $F_{freeze-out}$ values greater than 1000 are represented by a cross in panels (c) and (d).

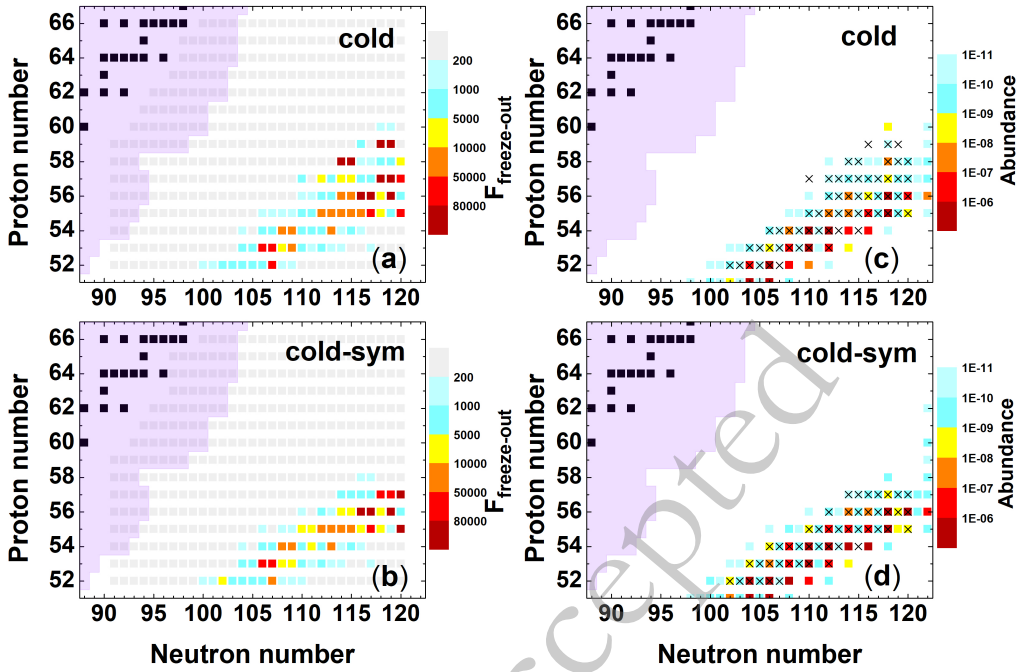

Fig. 4. (Color Online) Same as Fig. 3, but with results in the *cold* and *cold-sym* scenarios.

Here, we take the integrated fission flow $f_i^{(n)}$ of a parent nucleus n, multiply it by the fission yield $w_i(A)$ of the corresponding fission product with mass number A, and then sum the contributions from all fissioning nuclei, where i refers to a certain fission channel. The $\Delta Y_{Fragment}$ represents the increase in the abundance of nuclei with mass number A due to fission deposition. Details of the relevant physical quantities can be found in Ref. [29]. The calculated contribution of fission fragments to abundance is shown in Fig. 5. The results indicate that when using the GEF model, a significant number of fission fragments are distributed within the rare-earth peak mass region. In the *hot2* and *cold* scenarios, the overall abundance in the rare-earth peak region is very low at freeze-out. However, as nucleosynthesis progresses, a substantial amount of fission fragments is deposited in this region, gradually increasing abundance in the rare-earth region. The contribution of fission fragments diminishes the variations in the rare-earth peak abundance distribution that were initially caused by nuclear mass changes. As a result, the impact of mass variations in region I is masked by the distribution of fission fragments, leading to a generally lower sensitivity measure F for nuclei in this region. In contrast, under the *cold-sym* scenario, where a symmetric fission treatment is applied, fission fragments are only deposited near the second *r*-process peak, as indicated by the blue squares in Fig. 5. In the absence of a direct contribution of fission fragments to the rare-earth region, the differences in the abundance at freeze-out caused by mass variations in region I persist and ultimately influence the final rare-earth peak abundance distribution. So, the sensitivity of region I is increased again. However, the solar rare-earth peak abundance cannot be reproduced by using the symmetric fission treatment.

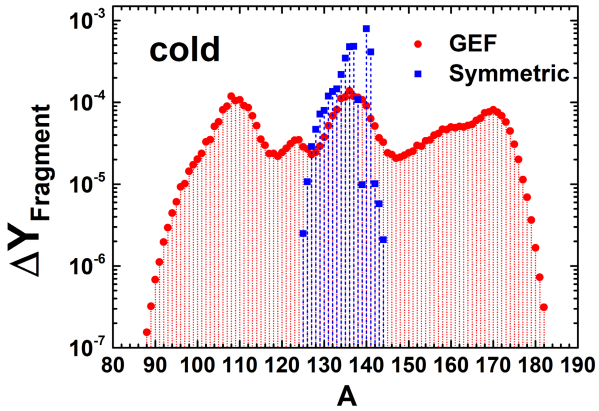

Fig. 5. (Color Online) Contribution of fission fragments to the abundance distribution in the *cold* scenario. The red dots represent the increase in abundance due to fission deposition when using the GEF fission fragment distribution model, while the blue squares represent the contribution of fission fragments under the simple symmetric fission treatment.

When the *r*-process nuclear flow reaches region II, the rare-earth peak is essentially fully formed, and its shape is highly sensitive to mass variations of nuclei in this region, which are located along the *r*-process path at the time when $\tau_{n\gamma} \approx 3\tau_{\beta}$. As mentioned above, in the *hot2* and *cold* scenarios, the contribution of fission products eliminates the high sensitivity of nuclei along the early *r*-process path (region I). However, in the process of nucle-

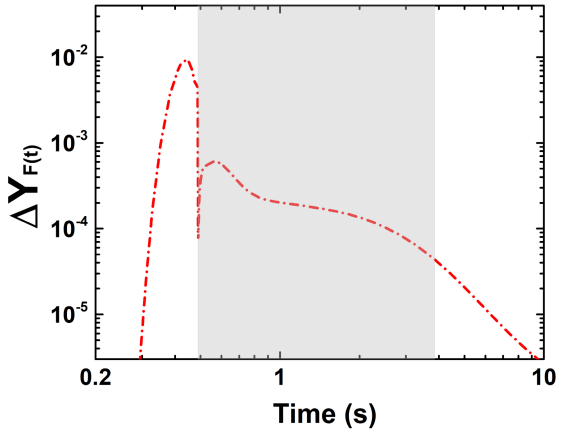

Fig. 6. (Color Online)Evolution of the contribution of fission fragments to the rare-earth peak abundances over time in the *cold* scenario. The shaded area represents the time interval for the formation of the rare-earth peak, from the time of *r*-process freeze-out to the time when the neutron capture timescale $\tau_{n\gamma}$ is approximately equal to 3 times the β-decay timescale τ_{β}.

ar flow decay back to stability, the fission flow will gradually decrease over time, which means that the contribution of fission fragments to the rare-earth peak abundance will gradually decrease. We calculated the contribution of fission products to rare-earth peak abundances over time in the *cold* scenario, as shown in Fig. 6. $\Delta Y_F(t)$ is defined as

$$\Delta Y_F(t) = \sum_{A=150}^{178} \sum_{n} \sum_{i} F_i^{(n)}(t) \times w_i(A), \tag{4}$$

where $F_i^{(n)}(t)$ is the fission flow of a parent nucleus n at a certain moment t, and $w_i(A)$ is the fission yield. We sum the contributions from all fissioning nuclei to the rare-earth mass region $A = 150 - 178$. The $\Delta Y_F(t)$ represents the increase in the abundance of nuclei with $A = 150 - 178$ due to fission deposition. The results show that after the *r*-process freeze-out, the contribution of fission to the rare-earth peak gradually decreases. For nuclei in region I, which are produced around the time of *r*-process freeze-out, the strong deposition of fission products begins to take effect at this stage and eventually erases the mass sensitivities. However, as the nuclear flow reaches region II at a later time, the contribution of fission gradually decreases, and hence the weakening effect of fission fragments on the difference of abundance distribution becomes weaker. Therefore, nuclei in region II still have larger F values. In addition, we note a distinct spike in the contribution of fission fragments at around 0.5 s in Fig. 6. This evolution closely follows the time-dependent behavior of the fission flow $F_i^{(n)}(t)$, and the observed feature results from two combined effects. First, the neutron-to-seed ratio drops rapidly and falls below 1.0 around the time of *r*-process freeze-out (~0.48 s). The sudden reduction in the free neutron population leads to a sharp decline in neutron-induced fission. After freeze-out, β-delayed neutron emission provides additional free neutrons, reviving the neutron-induced fission flow and contributing to the subsequent increase in the total fission flow. Second, β-delayed fission primarily occurs after freeze-out. As the relevant nuclei decay and undergo β-delayed fission, their contribution to the total fission flow becomes significant [29]. These two effects together lead to the second hump observed around 0.5 s in both the total fission flow and the contribution of fission fragments to the rare-earth peak abundances.

IV. SUMMARY

Based on the results of sensitivity studies in our previous work [24], we further analyzed the underlying reasons for the different distribution patterns of high-sensitivity nuclei across various astrophysical scenarios. The results show that mass variations of nuclei in region I (20-30 neutrons away from stability) have a significant impact on the abundance distribution at *r*-process freeze-out across all four scenarios, highlighting the universality of their influence at this stage. However, in scenarios with extensive fission activity, the subsequent deposition of fission products into the rare-earth region begins to take effect after freeze-out. Fission deposition effectively resets the local abundances in this region and suppresses the sensitivity to nuclear masses along the *r*-process freeze-out path. This process significantly reduces the uncertainty in the rare-earth peak abundances caused by mass variations in region I, producing a more robust *r*-process abundance distribution.

With time evolution, the fission flow in *r*-process nucleosynthesis gradually declines, leading to a reduced contribution from fission deposition. As the *r*-process path moves toward stability at a later time, the weakening effect of fission fragments on the difference in abundance distribution becomes weaker. Consequently, the sensitivity of nuclear masses in region II (7-15 neutrons away from stability) remains less affected by fission fragments, allowing nuclei in this region to retain relatively high sensitivity. This study highlights the impact of fission on the sensitivity of *r*-process abundances to nuclear masses, contributing to a better understanding of rare-earth peak formation and improving its effectiveness as a diagnostic for the *r*-process site.

References

[1] E. M. Burbidge, G. R. Burbidge, W. A. Fowler, and F. Hoyle, Rev. Mod. Phys. **29**, 547 (1957)
[2] K. Marti and H. D. Zeh, Meteoritics **20**, 311 (1985)
[3] J. J. Cowan, C. Sneden, J. E. Lawler, A. Aprahamian, M. Wiescher, K. Langanke, G. Martínez-Pinedo, and F.-K. Thielemann, Rev. Mod. Phys. **93**, 015002 (2021)
[4] X. D. Xu, B. Sun, Z. M. Niu, Z. Li, Y.-Z. Qian, and J. Meng, Phys. Rev. C **87**, 015805 (2013)
[5] D. Martin, A. Arcones, W. Nazarewicz, and E. Olsen, Phys. Rev. Lett. **116**, 121101 (2016)
[6] M. Mumpower, R. Surman, G. McLaughlin, and A. Aprahamian, Progress in Particle and Nuclear Physics **86**, 86 (2016)
[7] Z. Li, Z. Niu, and B. Sun, Science China Physics, Mechanics, and Astronomy **62**, 982011 (2019)
[8] T. M. Sprouse, R. Navarro Perez, R. Surman, M. R. Mumpower, G. C. McLaughlin, and N. Schunck, Phys. Rev. C **101**, 055803 (2020)
[9] J. Chen, J. Y. Fang, Y. W. Hao, Z. M. Niu, and Y. F. Niu, The Astrophysical Journal **943**, 102 (2023)
[10] Y.-W. Hao, Y.-F. Niu, and Z.-M. Niu, Phys. Rev. C **108**, L062802 (2023)
[11] R. Surman, J. Engel, J. R. Bennett, and B. S. Meyer, Phys. Rev. Lett. **79**, 1809 (1997)
[12] M. R. Mumpower, G. C. McLaughlin, and R. Surman, Phys. Rev. C **85**, 045801 (2012)
[13] M. R. Mumpower, G. C. McLaughlin, and R. Surman, The Astrophysical Journal **752**, 117 (2012)
[14] M. Mumpower, R. Surman, D. L. Fang, M. Beard, and A. Aprahamian, Journal of Physics G: Nuclear and Particle Physics **42**, 034027 (2015)
[15] M. R. Mumpower, R. Surman, D.-L. Fang, M. Beard, P. Möller, T. Kawano, and A. Aprahamian, Phys. Rev. C **92**, 035807 (2015)
[16] X. F. Jiang, X. H. Wu, and P. W. Zhao, The Astrophysical Journal **915**, 29 (2021)
[17] S. Brett, I. Bentley, N. Paul, R. Surman, and A. Aprahamian, The European Physical Journal A **48**, 184 (2012)
[18] A. Aprahamian, I. Bentley, M. Mumpower, and R. Surman, AIP Advances **4**, 041101 (2014)
[19] J. Beun, J. C. Blackmon, W. R. Hix, G. C. McLaughlin, M. S. Smith, and R. Surman, Journal of Physics G: Nuclear and Particle Physics **36**, 025201 (2008)
[20] R. Surman, J. Beun, G. C. McLaughlin, and W. R. Hix, Phys. Rev. C **79**, 045809 (2009)
[21] M. R. Mumpower, G. C. McLaughlin, and R. Surman, Phys. Rev. C **86**, 035803 (2012)
[22] Surman, R., Mumpower, M., Ca ss, J., Bentley, I., Aprahamian, A., and McLaughlin, G. C., EPJ Web of Conferences **66**, 07024 (2014)
[23] M. Mumpower, J. Cass, G. Passucci, R. Surman, and A. Aprahamian, AIP Advances **4**, 041009 (2014)
[24] Y. W. Hao, Y. F. Niu, and Z. M. Niu, Physics Letters B **844**, 138092 (2023)
[25] https://sourceforge.net/projects/nucnettools/, .
[26] P. Moller, J. Nix, W. Myers, and W. Swiatecki, Atomic Data and Nuclear Data Tables **59**, 185 (1995)
[27] https://tendl.web.psi.ch/tendl2019/talys.html, .
[28] https://reaclib.jinaweb.org/, .
[29] Y. W. Hao, Y. F. Niu, and Z. M. Niu, The Astrophysical Journal **933**, 3 (2022)
[30] http://www.cenbg.in2p3.fr/GEF, .
[31] N. Vassh, R. Vogt, R. Surman, J. Randrup, T. M. Sprouse, M. R. Mumpower, P. Jaffke, D. Shaw, E. M. Holmbeck, Y. Zhu, and G. C. McLaughlin, Journal of Physics G: Nuclear and Particle Physics **46**, 065202 (2019)
[32] M. Wang, W. Huang, F. Kondev, G. Audi, and S. Naimi, Chinese Physics C **45**, 030003 (2021)
[33] C. Sneden, J. J. Cowan, and R. Gallino, Annual Review of Astronomy and Astrophysics **46**, 241 (2008)